Cooling Precipitation and Strengthening Study in Powder Metallurgy Superalloy U720LI

JIAN MAO, KEH-MINN CHANG, WANHONG YANG, KOUSHIK RAY, SUHAS P. VAZE, and DAVID U. FURRER

The excellent mechanical properties of powder metallurgy (P/M) superalloys strongly depend on the microstructure, such as grain size, and morphology and size distribution of the γ' precipitates. The microstructure is, in turn, determined by the heat treatment, *viz.*, solution annealing, quenching, and subsequent aging. To study the effect of the quenching process, two types of quenching methods were used to produce different quenched microstructures in a UDIMET 720LI (U720LI) alloy. One was a continuous quenching method, where samples were cooled along linearly controlled cooling profiles, each at a fixed cooling rate. This test studied the effect of cooling rate on the size of cooling γ' precipitates (formed during quenching) and the consequent strengthening effect. The other test was the interrupted quenching test, which allowed tracking the growth of cooling γ' precipitates with decreasing temperature during quenching at a given cooling rate. The strengthening response at each interrupt temperature was also studied. Results from the continuous cooling tests showed that the relationship between the size of the cooling γ' precipitate and the cooling rate obeys a power law, with an exponential being about 0.35. The tensile strength was found to increase linearly with the cooling rate. Strengthening due to the subsequent aging treatment occurred regardless of cooling rates. The interrupted cooling tests showed that γ' growth is a linear function of decreasing temperature for a given cooling rate. A nonmonotonic degradation of tensile strength against interrupt temperature was discovered.

I. INTRODUCTION

THE excellent high-temperature strength of powder metallurgy (P/M) superalloys is mostly due to the precipitation of ordered and coherent γ' (Ni_3Al) phase from the solid-solution matrix, besides some solid-solution strengthening in the γ matrix. Control of γ' precipitation through heat treatment is critical to the final mechanical properties, because the nucleation and growth kinetics of the precipitates strongly depend on the cooling rate during quenching. If the cooling rate is fast enough to avoid or limit the formation and growth of extensive cooling γ' precipitates, a high density of fine γ' precipitates can be subsequently developed to achieve desirable properties. Therefore, higher cooling rates result in higher strength.[1] However, the strength gained from fast quenching would be limited by the possibility of quench cracking or severe shape distortion due to the high thermal stresses induced.[2–6]

Numerous efforts have been directed at simulating the relationship between the cooling rate and the resultant mechanical properties, as mentioned previously.[7–12] The problem with accurately characterizing this relationship is associated with the description of the cooling rate itself. Traditional cooling-rate studies were mostly conducted by quenching a component in a bath after holding it at the solution temperature. Thus, the cooling profile depended on the heat-transfer coefficient of the quenchant, which varied as a function of decreasing temperature during quenching. Another method for obtaining different cooling rates was the Jominy bar test, which yielded different cooling profiles at different points along the length of the quenched bar.[13] In this case too, the cooling rates varied as a function of temperature. Therefore, an average cooling rate for the entire process (or for a given temperature range) was adapted as the cooling parameter. In practice, the size of the precipitates depends on the actual cooling profile, which varies not only with quench procedure, but also with the configuration of the component, the heat-transfer coefficient, and the cooling characteristics of the quenchant.[14,15] As a result, using an average cooling rate within a temperature range can only produce an approximate relationship between the size of cooling γ' precipitates and the cooling rate.

The main objective of this research is to develop an empirical model that would be capable of predicting the size of the quenched γ' precipitates and their strength, as a function of cooling rate, in a superalloy component. The advantage of this work is the ability to precisely control the linear cooling profile and then to develop a real correlation between the cooling rate and γ' precipitate size. This study will provide valuable input to the thermal process simulation on optimizing thermal process parameters for specific requirements of a given P/M superalloy component.

II. EXPERIMENTAL INVESTIGATION

A. *Material*

The P/M UDIMET 720LI (U720LI) material used in this investigation was cut from the rim of a disk provided by Ladish Co. Inc. The U720LI alloy contains lower C, B, and Cr contents than the original version of U720. The disk

JIAN MAO, Postdoctoral Student, KEH-MINN CHANG, Professor, and WANHONG YANG, former Research Assistant Professor, are with the Department of Mechanical and Aerospace Engineering, West Virginia University, Morgantown, WV 26505. KOUSHIK RAY, Engineer, and SUHAS P. VAZE, Manager, are with Concurrent Technologies Corporation, Johnstown, PA 15904. DAVID U. FERRER, Manager, is with Ladish Co., Inc., Cudahy, WI 53110.

Manuscript submitted November 15, 2000.

Table I. Compositions of P/M Superalloy U720LI

Alloy	C	S	W	Mo	Zr	Co	Al	Cr	Ti	Fe	Ni
U720LI	0.025	0.005	1.3	3.02	0.035	14.75	2.46	16.35	4.99	0.06	Bal

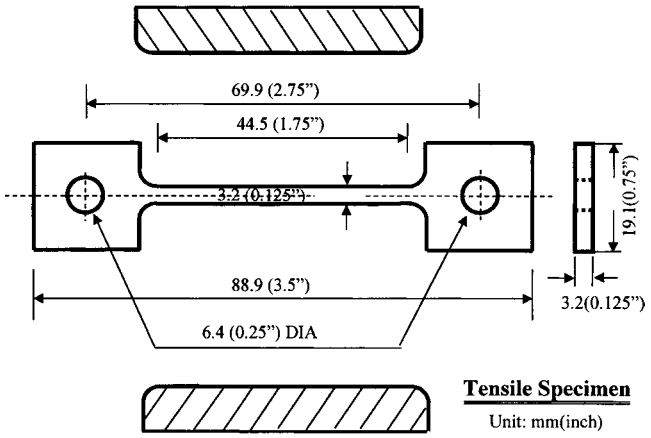

Fig. 1—Specimen drawing for tensile test and metallography examination.

was produced by the standard manufacturing route of alloy atomization, hot compaction, extrusion, and isothermal forging. The diameter of the disk is 660 mm, and the thickness at the rim is 48 mm. Samples were cut from the rim of the disk in the tangential direction. The chemical composition of the material is given in Table I.

B. *Continuous and Interrupted Cooling Tests*

Sheet blank specimens for the cooling test were cut by a wire electrolytic-discharge machine (EDM) to a size of about $19 \times 3.2 \times 89$ mm, as shown in Figure 1. Tensile specimens were also machined by the EDM from the quenched blanks into dog-bone shapes. The cut-off parts, identified in Figure 1 by hatched lines, were used for the metallography examination.

Differential thermal analysis (DTA) was combined with the thermodynamic simulation to determine the phase transition temperatures. The DTA test was conducted using a TA Instruments DTA 1600 furnace. The heating\cooling rate during the test was 2 °C/min. The thermodynamic process of the phase transformation was simulated using Thermo-Calc software, Version M, in conjunction with the 13 elements Ni-Fe database, developed by Royal Institute of Technology (Stockholm, Sweden).

All cooling tests were performed using a unique computer-controlled quenching system, equipped with a high-power quartz heater, a data acquisition board, a power controller, and a temperature controller. The temperature capability of the furnace is 1260 °C, and the maximum cooling rate was about 1055 °C/min. The other features of this system are as follows:

(1) accurate control of the linear cooling/heating profile through the entire process over the desired temperature range;
(2) real-time multichannel temperature display;
(3) time and temperature data acquisition at a specified sampling rate;
(4) on-cooling data tracking for examining practical cooling profiles; and
(5) multistep cooling-path control mode to examine various cooling patterns.

1. *Continuous cooling tests*

These tests were aimed at studying the effect of a linear, fixed cooling rate on the size of the cooling γ' precipitates. Specimens were heated to a supersolvus solution temperature of 1175 °C, held for 5 minutes (based on the study of grain-size growth kinetics[16]), and then quenched at a controlled cooling rate. Six different cooling rates—11 °C/min, 27 °C/min, 55 °C/min, 110 °C/min, 167 °C/min, and natural cooling at 800 °C/min—were selected. These cooling rates were representative of the range of cooling rates encountered by the material during quenching of typical superalloy turbine disks. The cooling rates were controlled from the supersolvus temperature of 1175 °C down to 650 °C. On reaching 650 °C, the specimens were rapidly quenched by turning off the power (also referred to as natural cooling hereafter). Natural cooling was achieved by turning off the power of the quartz heater after the solution holding time. Note that the heat was lost by natural convection and conduction through the water-cooled grips after turning off the power. The cooling rate was not well controlled, but was found to be nearly linear within the temperature range of interest. For each test, the cooling profile was recorded by a computer using a pair of thermocouples spot-welded onto the two faces of each specimen.

2. *Interrupted cooling tests*

These tests were designed to lead to a better understanding of the development of the cooling precipitates and precipitation kinetics. The interrupted cooling test was comprised of several continuous cooling tests, each interrupted at a different intermediate temperature. Tests were carried out by heating the specimens to a supersolvus solution temperature of 1175 °C, holding for 5 minutes, and then quenching at 55 °C/min. The cooling was interrupted at 1121 °C, 1065 °C, 1010 °C, 954 °C, and 899 °C, respectively, and the specimens were then quenched rapidly from these temperatures by turning off the power, as described before.

C. *Examination of the Cooling Precipitates*

After each cooling test, a sample was taken from the center of the part cut off from the quenched blank (refer to the hatched region in Figure 1) for metallography. The samples were manually ground to 800 grit on a Handimet2 roll grinder, electrolytically polished, and electrolytically etched. After each step, the samples were rinsed in methanol and then blow-dried to avoid stains. The γ' phase was easily highlighted in the samples prepared in this manner. The key to sample preparation for the precipitate-size measurement is to assure that only one layer of γ' on the surface is etched and that there is no overlapping of the particles. Sample preparation procedures are summarized in Table II.

Table II. Sample Preparation Schedule

	Enchant Solution	Voltage, *v*	Time, s	Phase
Electrolytic polishing	80 pct methanol + 20 pct HCL	25 to 30	15	—
Electrolytic etching	170 mL H_3PO_4 + 16 g CrO_3 + 10 mL H_2SO_4	3 to 5	2 to 3	γ'

Cooling precipitates were examined using a JEOL*-6400 scanning electron microscope (SEM). The operating voltage was 20 kV and the current of the condenser lens was 0.06 nA. The magnification was between 10 and 50 kX.

*JEOL is a trademark of Japan Electron Optics Ltd., Tokyo.

D. *Image Processing and Statistical Analysis*

Images were processed and analyzed using ScionImage and MICROSOFT EXCEL.* ScionImage is a public-domain software from the National Institutes of Health (www.nih.gov). Before using ScionImage software, SEM pictures were manually optimized to enhance the boundary contrast between the γ' particles and the matrix. The size of each particle was taken to be the diameter of a circle with the same area as the particle, designated as the equivalent circle diameter. In order to ensure the accuracy of statistical analysis, the total number of particles counted in each specimen was between 200 and 1000. The mean diameter and size distribution of the particles were statistically analyzed using descriptive analysis and histogram analysis in MICROSOFT EXCEL.

*MICROSOFT EXCEL is a trademark of Microsoft Corporation, Redmond, WA.

The cooling precipitates referred to here are defined as the precipitates formed during the quenching (cooling). In statistical analysis, only those cooling precipitates with a size larger than 0.05 μm were counted, according to the SEM resolution.

E. *Mechanical Property Tests*

Room-temperature tensile tests were performed on specimens from both the continuous and interrupted cooling tests in the as-quenched and aged status. For the continuous cooling test, as-quenched samples were produced by cooling specimens from a solution temperature of 1175 °C to 650 °C at 27 °C/min, 55 °C/min, 111 °C/min, and 167 °C/min, respectively. The holding time at the solution temperature was 5 minutes. The tensile data from as-quenched specimens were then compared with the data obtained from identical (same cooling history) samples that were additionally aged at 700 °C for 24 hours and then air cooled. Tensile tests were also performed on the as-quenched specimens that were prepared after interrupting a 55 °C/min (100 °F/min) cooling test at 1175 °C, 1121 °C, 1065 °C, 1010 °C, 954 °C, and 650 °C, respectively.

The geometry of the tensile specimen has already been shown in Figure 1. Tensile tests were performed using a computer-controlled MTS machine supported by LABVIEW* software. The strain rate for the tensile tests was 0.0024 min^{-1}.

*LABVIEW is a trademark of National Instruments, PA.

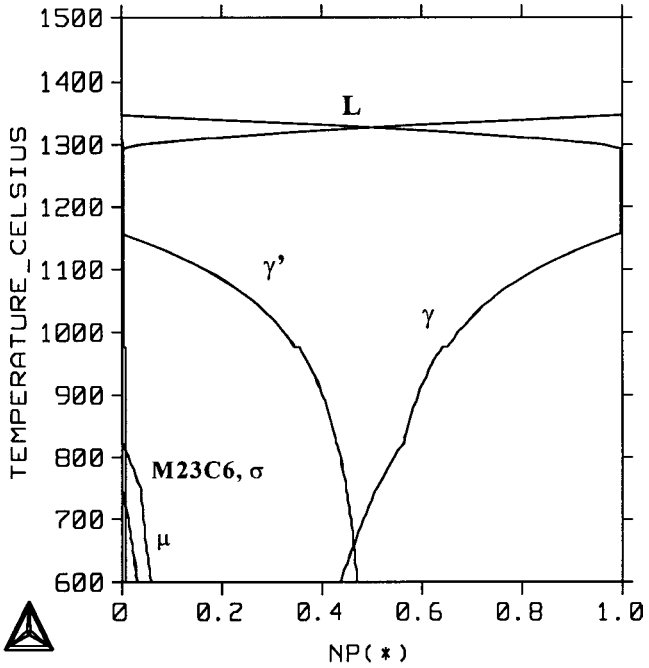

Fig. 2—Phase diagram of UDIMET 720LI alloy predicted by Thermo-Calc.

Table III. Key Thermodynamic Data of U720LI

Alloy	Liquidus	Solidus	γ' Solvus	γ' Molar Fraction at 700 °C	Heat Treatment Window
U720LI	1340 °C	1290 °C	1153 °C	0.44	142 °C

III. RESULTS

A. *Phase-Transformation Analysis and γ' Solvus Temperature Determination*

Figure 2 shows the equilibrium phase diagram of U720LI calculated by using Thermo-Calc. According to the diagram, the γ' solvus temperature is about 1153 °C and the γ' volume fraction at the aging temperature of 700 °C is about 0.44, which is the maximum volume fraction available after aging.

According to the DTA test, the γ' solvus temperature was measured to be 1145 °C for U720LI, which is comparable to that predicted by Thermo-Calc (1153 °C). The difference between the incipient melting temperature and the γ' solvus temperature, called the "heat-treatment window," is another important parameter in the control of the supersolvus heat-treatment process. The window was also measured from the DTA test results, which is found to be about 142 °C for the U720LI alloy. Some important thermodynamic data of U720LI alloys are summarized in Table III.

In any controlled cooling test, the equilibratory nucleation and growth of precipitates are suppressed due to fast cooling.

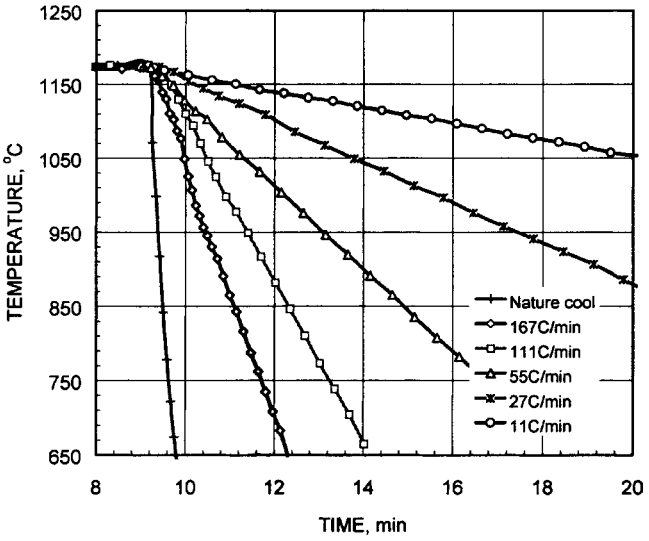

Fig. 3—Cooling curves of U720LI alloy.

Table IV. Comparison of Preset Cooling Rates and Measured Cooling Rates

	Cooling rate, °C/min					
Preset	11	27	55	111	167	nature cooling
Measured	11.0	27.6	56.5	110.2	171.6	800.3

The variation of the nonequilibrium γ' amount against temperature at a given cooling rate can be experimentally estimated with the interrupted cooling test. By comparing the equilibrium phase diagram and phase volume fractions from the nonequilibrium cooling studies, the supersaturation of the matrix as a function of temperature and cooling rate can be characterized, which will provide valuable data for future work on precipitation simulation studies.

B. *Continuous Cooling Precipitation*

1. *Cooling Curves*

Recorded linear cooling curves from continuous cooling tests are shown in Figure 3. The linear controlled cooling profiles are as expected. The comparison of the preset cooling rates and the real cooling rates obtained from data fitting is listed in Table IV. The ability of the control system to maintain preset cooling rates over a wide range is clearly demonstrated.

2. *Effect of cooling rate on cooling precipitation*

During supersolvus solution treatment, all the primary γ' precipitates remained after forging were dissolved. As the temperature decreased from the solution temperature, upon cooling, some γ' started to precipitate from the matrix. Those precipitates that formed during the quenching process are defined as cooling precipitates. The morphology and the size distribution of the cooling precipitates strongly depend upon the cooling rate.

a. *Morphology of the cooling precipitates*

The morphology of the cooling precipitates in the U720LI alloy varies with cooling rate, as shown in Figure 4. Cooling precipitates were uniformly distributed in the matrix; large blocky cooling precipitates accompanied by very fine precipitates were also found along grain boundaries (Figure 5). With the decrease in cooling rate, the sizes of the homogeneously distributed cooling precipitates became larger, and their shapes changed from somewhat cuboidal to somewhat irregular ones.

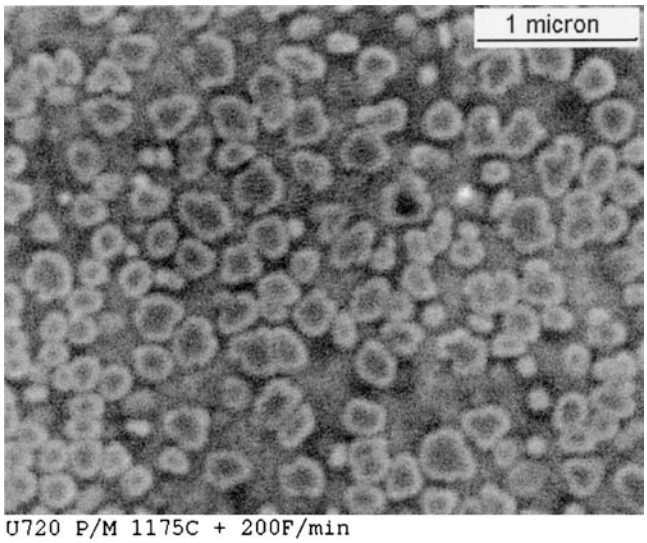

(*a*) Solution temperature: 1175°C, cooling rate: 111°C/min

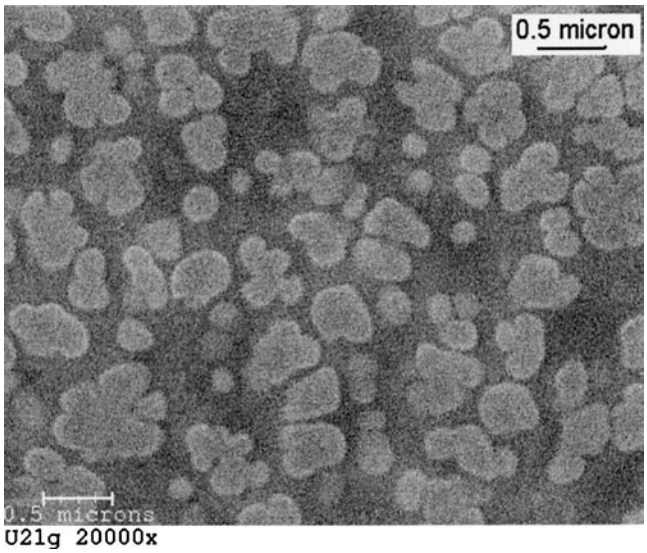

(*b*) Solution temperature: 1175°C, cooling rate: 11°C/min

Fig. 4—(*a*) and (*b*) The morphology of cooling precipitates varied with cooling rates.

b. *Precipitate size vs cooling rate*

An empirical modeling of precipitation of γ' was developed to characterize the relationship between the size of cooling precipitates and cooling rate. The size of a cooling precipitate is characterized by the equivalent circle diameter in the statistical analysis, as mentioned previously. The mean size of cooling precipitates as a function of cooling rate is plotted in Figure 6. Because the precipitates from the natural cooling were too small to be counted, no data point was included. The statistical results are summarized in Table V. The cooling precipitates in the U720LI alloy had an average diameter of about 0.15 to 0.35 μm over the cooling-rate

range of 167 °C/min to 11 °C/min. As the cooling rate decreases, the size and the volume fraction of cooling precipitates increase, which has been previously shown in several other alloys.[8,10,12] However, at a cooling rate of 27 °C/min, the mean size of cooling precipitates actually decreases and shifts away from the trend line. The mean size increases again when the cooling rate decreases to 11 °C/min. To explain this phenomenon, a histogram analysis of the particle size was carried out, shown in Figure 7. In the legends of Figure 7, "frequency" is defined as the percentage of particles with diameters within an interval range, and "cumulative pct" means the percentage of particles with a diameter smaller than the given value.

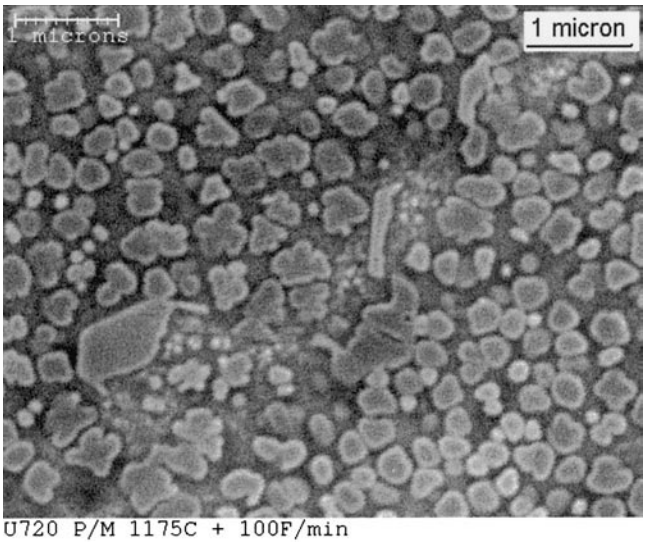

Fig. 5—Distribution of the cooling precipitates on grain boundary.

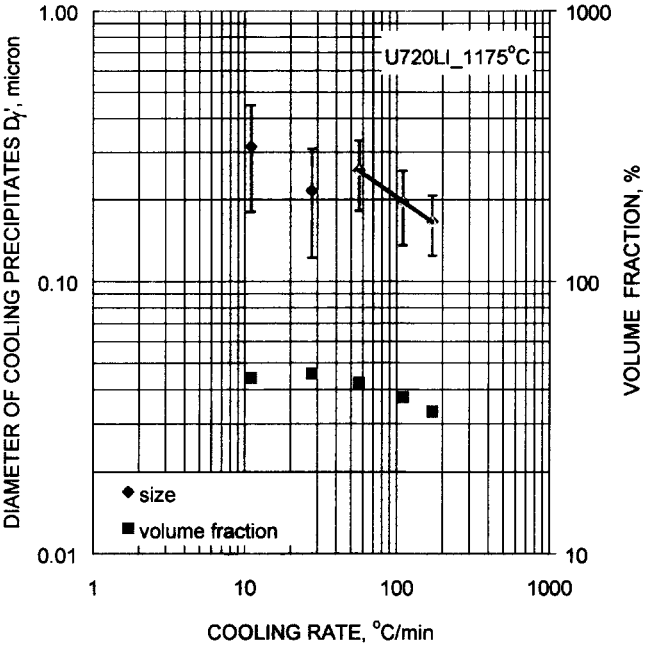

Fig. 6—Plot of cooling precipitate size and volume fraction against cooling rate.

It is observed that the mean diameter of the precipitates increases with decreasing cooling rate, *i.e.*, the peak size corresponding to the highest frequency moves toward a larger value. Also, the histograms show a normal distribution of the frequency. Note that when the cooling rate is higher than 55 °C/min, only a single peak is observed. However, for cooling rates below 27 °C/min, the size distribution shows two peaks. This is believed to be due to a second round of precipitate nucleation during quenching, here onward referred to as secondary-burst precipitates. The secondary-burst precipitates are much smaller than the primary ones. This binomial distribution brings down the average size of the cooling precipitates. Hence, the discrepancy in the trend of cooling precipitate size at cooling rates lower than 27 °C/min is depicted in Figure 6.

In order to give an experimental correlation between the precipitate size and cooling rate, the effect of the smaller-sized secondary-burst precipitates on the average size was eliminated. This was done by identifying the crossover point in the bimodal distributions at low cooling rates and recalculating the average size of just the first-burst precipitates with only those precipitates whose size was larger than the crosspoint value. After this recalculation, the relationship between the size of first-burst cooling precipitates and cooling rate follows a normal power law with an exponent of about 0.35, as shown in Figure 8 and given subsequently:

$$\log D_{\gamma'} = 0.0165 - 0.354 \cdot \log (dT/dt) \text{ with } R^2 = 0.998 \quad [1]$$

where the precipitate diameter ($D_{\gamma'}$) is in microns, and the constant cooling rate (dT/dt) is in °C/min.

C. *Precipitation Modeling by Interrupted Cooling*

The interrupted cooling test, described previously, was conducted only at one cooling rate, namely, 55 °C/min (100 °F/min). The temperatures at which the test was interrupted were specified earlier. The growth kinetics of cooling precipitates was characterized by the variation of the cooling precipitate size with interrupt temperature. The recorded

Table V. Statistical Results of Measured Cooling Precipitate Size for Different Cooling Rates

Specimen Cooling Rate		Before Separation		After Separation		
ID	(°C/min)	Mean Diameter, μm	Standard Deviation	Mean Diameter, μm	Standard Deviation	Volume Fraction Pct
U702a	171.6	0.166	0.041	0.166	0.041	33.3
U703b	110.2	0.196	0.060	0.196	0.060	37.5
U704c	56.5	0.256	0.075	0.256	0.075	42.5
U706d	27.6	0.216	0.093	0.319	0.051	45.8
U721g	11.0	0.314	0.134	0.440	0.080	44.1

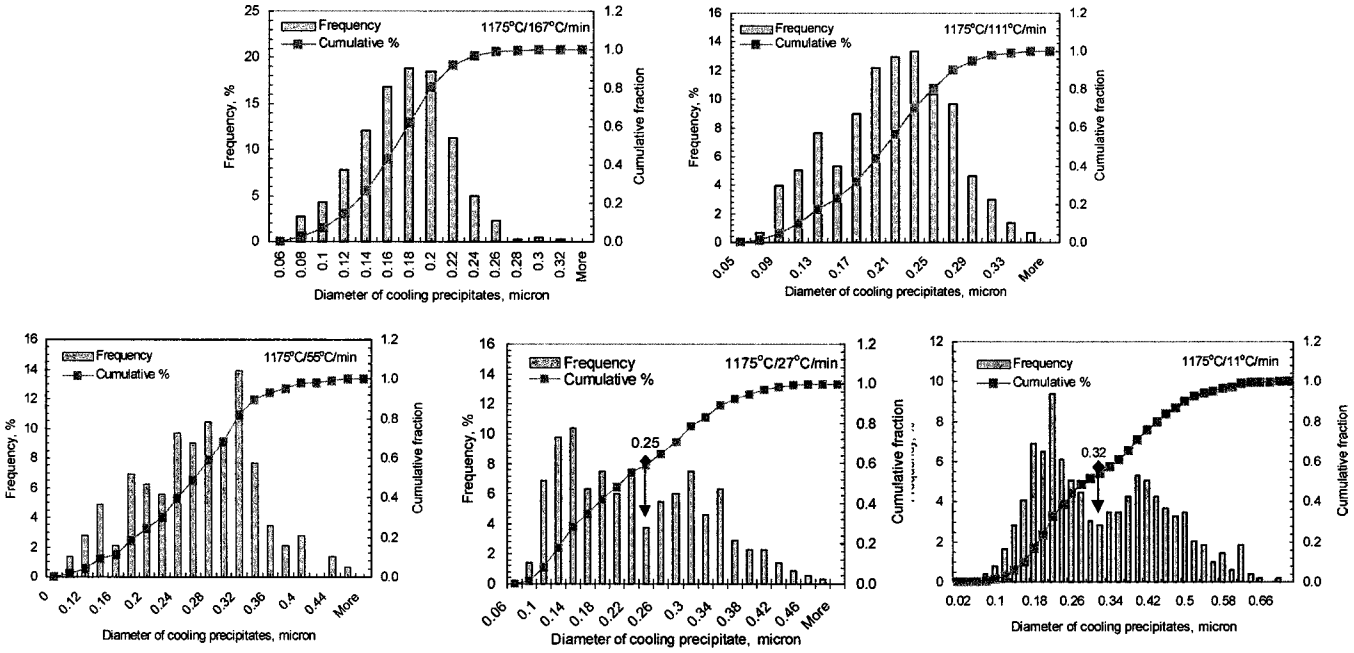

Fig. 7—Size distribution of cooling precipitates varies with cooling rate.

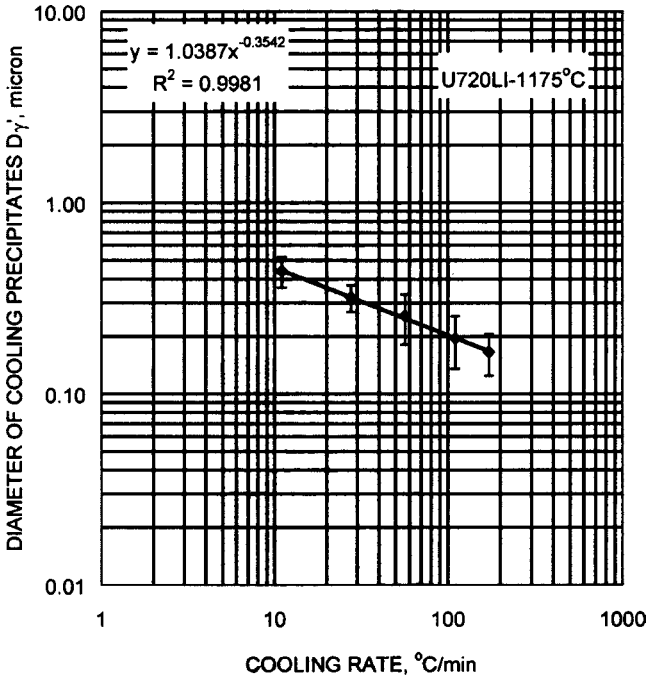

Fig. 8—Modified cooling precipitates size *vs* cooling rate (leave out the secondary burst γ').

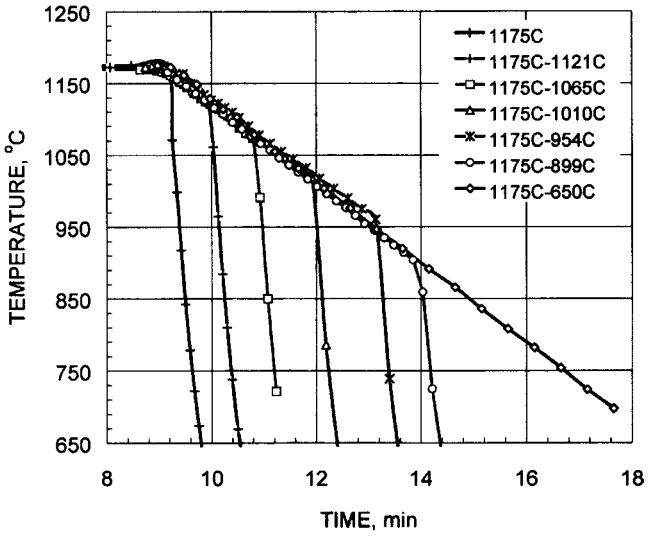

Fig. 9—Cooling curves during interrupt tests. Cooling rate before interruption: preset 55 °C/min, measured 56.7 °C/min; and cooling rate after interruption: 780 °C/min.

interrupted cooling curves are shown in Figure 9. The rapid quench after the interruption is an attempt to "freeze" the microstructure at the temperatures of interest.

1. *Cooling precipitates observation*

When the temperature falls below the γ' solvus from the solution temperature, γ' precipitates start to nucleate. The variation of cooling precipitate morphology with interrupt temperature is illustrated in Figure 10. At the studied cooling rate, the first cooling precipitates formed are mostly spherical and cuboidal in shape, with an average size of about 0.16 μm at 1121 °C. When the temperature drops to about 900 °C, irregular-shaped precipitates develop. The morphology change is believed to be associated with the coarsening or coalescing of the precipitates.

2. *Growth kinetics of cooling precipitates*

The average size of cooling precipitates as a function of interrupt temperature is plotted in Figure 11. Notice that the average size of first-burst particles actually remains almost stable at the beginning of the quench, until around 1065 °C. Below 1065 °C, the average size of precipitates starts to increase. The significant increase of the volume fraction actually occurs at a temperature below 1010 °C. As the temperature decreases further, the volume fraction of particles drops abruptly even as the average size of the particles continues

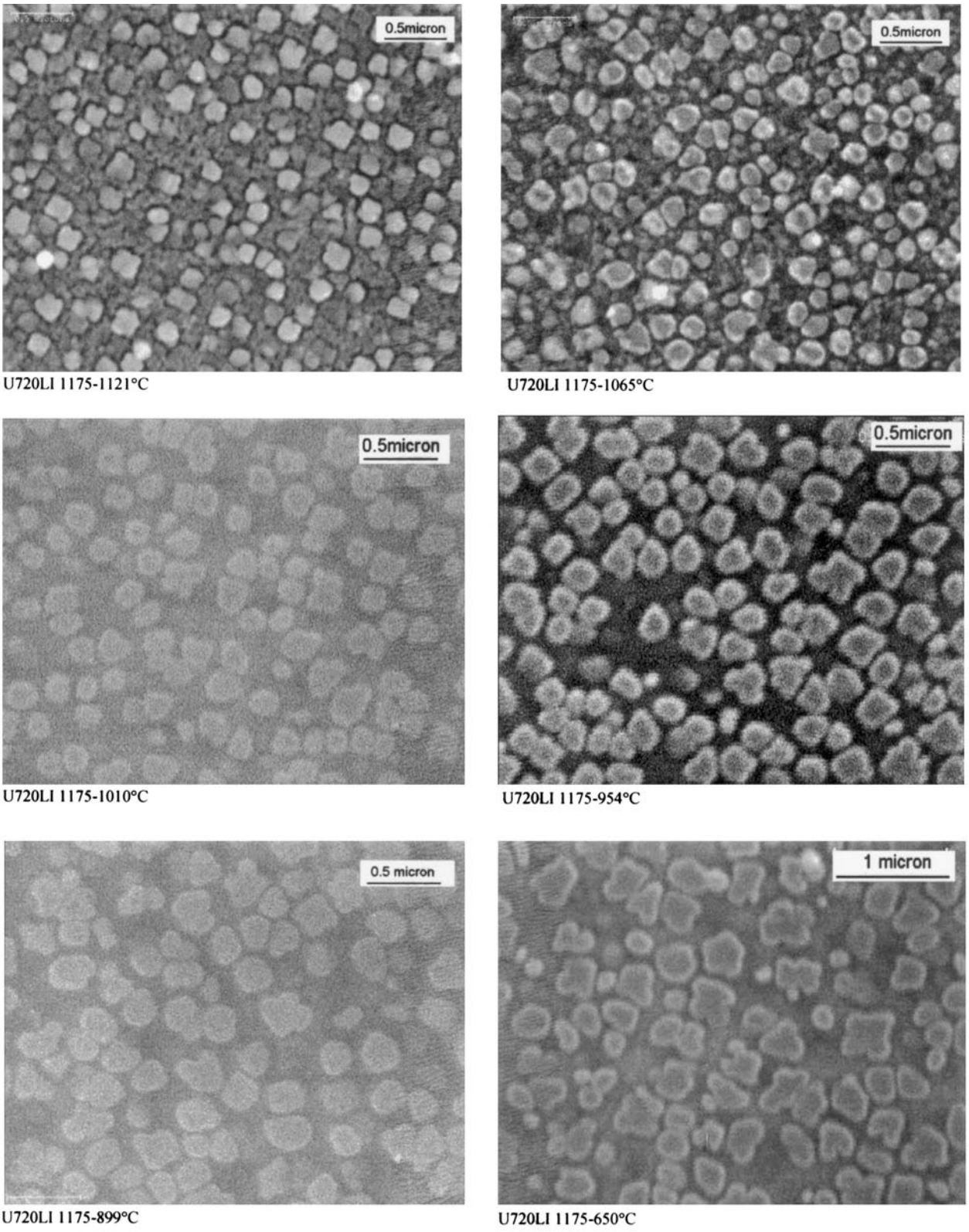

Fig. 10—Morphology of the cooling precipitates at the different temperature stages during cooling.

to increase. The growth kinetics of cooling precipitates can be expressed as a linear function of temperature, given as

$$D_{\gamma'} = -2.24 \cdot 10^{-4} T + 0.397 \quad \text{with} \quad R^2 = 0.96 \quad [2]$$

where the average precipitate diameter is in microns, and the temperature is in degrees Celsius.

From Figure 11, the relatively stable average precipitate size at the early stage of the quenching is believed to be

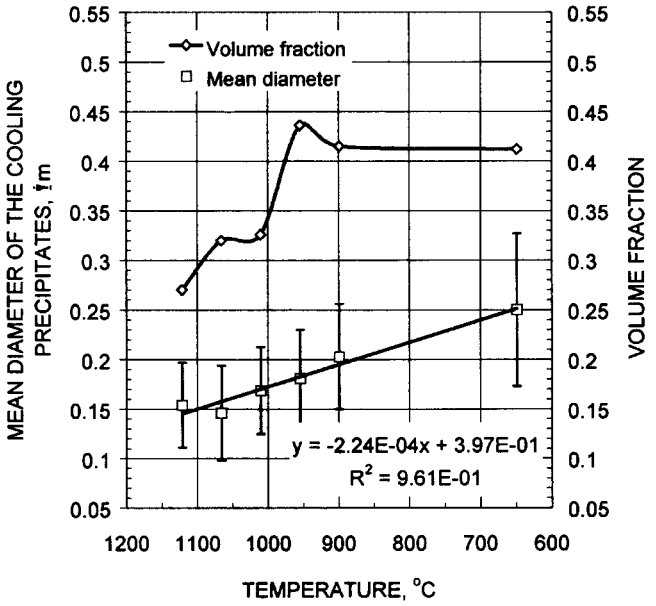

Fig. 11—Variation of the size and the volume fraction of cooling precipitate with the interrupt temperatures.

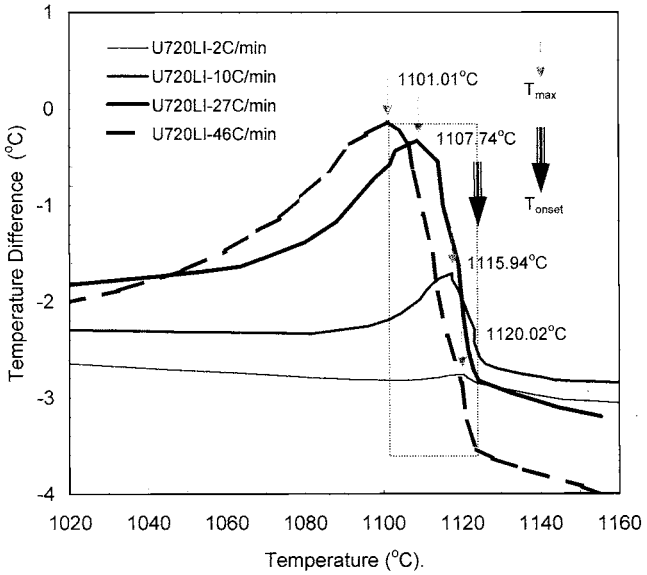

Fig. 12—Variation of undercooling and precipitation range with cooling rate, DTA.

related to the continuous formation of the γ' precipitates, which are considered to be the first-burst cooling precipitates. The γ' burst temperature is lower than the γ' solvus temperature, *e.g.*, under a certain undercooling, which is understandable based on the thermodynamic theory of nucleation and is also pointed out in another study.[17] The start temperature of the γ' burst is defined as the onset precipitation temperature (T_{onset}). Figure 12 shows the variation of T_{onset} and the γ' maximum precipitation temperature (T_{max}), corresponding to the maximum γ' precipitation rate, with cooling rate obtained from DTA tests. With the increase of the cooling rate, T_{onset} stays almost the same. However, T_{max} decreases with the increase of cooling rate. Consequently, the temperature range for precipitation (named the precipitation

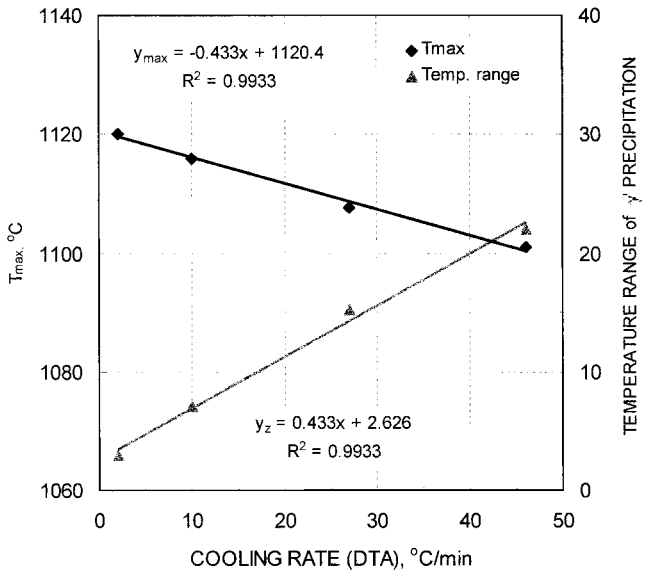

Fig. 13—Maximum precipitation temperature and temperature range as a function of cooling rate.

range, from T_{onset} to T_{max}) becomes wider, which means that the precipitation actually spans over a wide temperature range as the cooling rate increases. Observing the unchanged T_{onset} value can eliminate the effect of thermal inertia on the shift of the T_{max} value. It is interesting to note that both T_{max} and the magnitude of the precipitation range vary linearly with cooling rate (Figure 13), which are given as

$$T_{max} = -0.433 \cdot (dT/dt) + 1120.4 \quad \text{with} \quad R^2 = 0.99 \qquad [3]$$

$$\Delta T = T_{max} - T_{onset} = 0.433 \cdot (dT/dt) + 2.626 \quad \text{with} \quad R^2 = 0.99 \qquad [4]$$

where the cooling rate is in °C/min, and the temperature is in degrees Celsius.

At the cooling rate of 55 °C/min, the temperature at which maximum precipitation takes place is around 1096 °C, based on an extrapolation. The precipitation range is from 1150 °C to 1096 °C, an undercooling of 54 °C. Because of the existence of the precipitation range due to the undercooling where nucleation dominates, the average size of the precipitates remain relatively stable within that temperature range. As the temperature falls below the precipitation range, the growth of γ' dominates the cooling process and the average size of the cooling γ' starts to increase.

In addition, Figure 14 shows the variation of the precipitate densities with the interrupt temperature. There are two jumps in the precipitation density with the decrease of the interrupt temperature, which is consistent with the volume-fraction variation. This is believed to be due to the bimodal precipitation, as explained earlier, but further confirmation is needed. The decrease of the precipitation density is related to the coarsening of the precipitates, which coincides with the decrease in volume fraction.

D. *Mechanical Property*

1. *Effects of the cooling rate*

The measured yield strength and ultimate strength as a function of cooling rate is plotted in Figure 15. The cooling

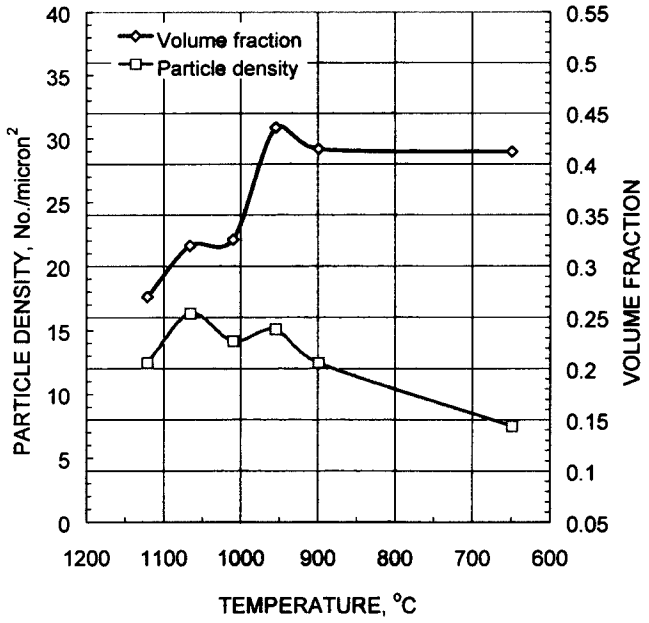

Fig. 14—Variation of precipitation density with the interrupt temperature.

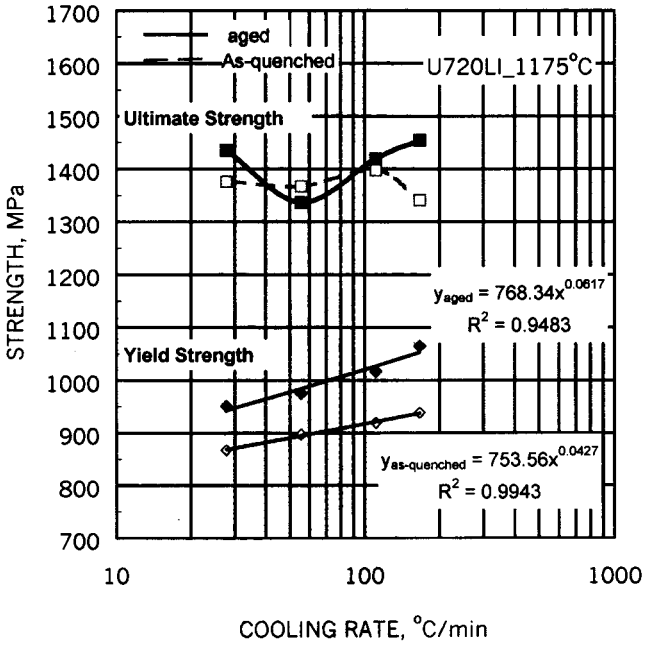

Fig. 15—Relationship between the tensile strength and cooling rates.

rate has a significant influence on the as-quenched yield strength of the material, but not much effect on the ultimate tensile strength. The yield strength is known to be more microstructure dependent and increases with cooling rate. It is expected that the highest cooling rate, even though producing very small γ' precipitates, results in the highest as-quenched tensile strength. In practice, the gain in strength through the cooling rate is only limited by the potential risk of quench cracking and distortion due to excessive thermal stresses generated during the quench. The yield strength of as-quenched specimens as a function of cooling rate can be correlated as an empirical equation, which follows a power law and is given as

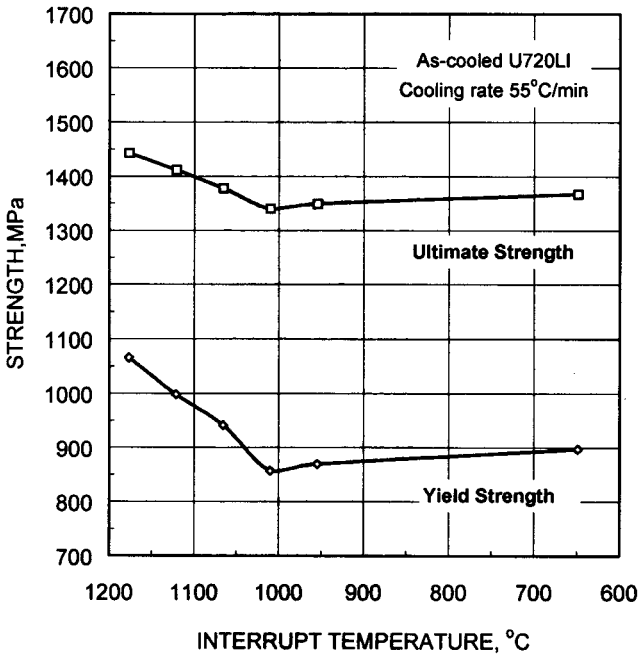

Fig. 16—The plot of as-quenched yield and tensile strength against the interrupt temperature.

$$\log \sigma_y = 2.877 + 0.0427 \cdot \log (dT/dt) \quad \text{with} \quad R^2 = 0.99 \qquad [5]$$

where the as-quenched yield strength (σ_y) is in mega Pascals, and the cooling rate is in °C/min.

After the single aging treatment (700 °C/24 hours then air cooled), all specimens, irrespective of cooling rates, show a marked improvement in the yield strength compared to the as-quenched specimens. The improvement is about 90 to 130 MPa, for cooling rates from 27 °C/min to 167 °C/min. The aged yield strength can also be approximated from the cooling rate by the following fitting equation:

$$\log \sigma_y = 2.886 + 0.0617 \cdot \log (dT/dt) \quad \text{with} \quad R^2 = 0.95 \qquad [6]$$

where aged yield strength is in mega Pascals, and the cooling rate is in °C/min.

However, Eq. [6] should only be applied to U720LI samples with an identical age treatment. Moreover, it is noted from Figure 15 that a higher cooling rate results in more aging strengthening than a lower cooling rate, because a faster quench produces more extensive fine γ' precipitates thereafter.

2. *Effect of the interrupt temperature*

Figure 16 shows a plot of the as-quenched yield strength against interrupt temperature (a fixed cooling rate of 55 °C/min). The first point (leftmost) on the plot corresponds to the data from the direct quenching from the solution temperature. The rightmost point corresponds to the data from the single cooling-rate test with a controlled cooling rate of 55 °C/min, which was interrupted at 650 °C. Comparing these two points, it is noted that the strength actually decreases after a controlled quenching. This decrease is further found to be nonmonotonic. Figure 16 shows the as-quenched yield strength against the interrupt temperature. When specimens

were interrupted at the early stages of the control cool, both the yield strength and ultimate strength decreased with the interrupt temperatures. However, as the interrupt temperature further decreased to about 1010 °C, the strength started to increase somewhat. But it never reached the value obtained from direct quenching from the solution temperature.

IV. DISCUSSION

A. *Precipitation Thermodynamics*

There are three stages of γ' precipitate formation during the entire cooling process: nucleation, growth, and coarsening. At a very high cooling rate, γ' nucleation actually might be suppressed, but it is almost impossible unless the cooling rate is higher than 10^4 K/min.[18] According the classic nucleation theory, the stable critical nucleus size is given by[19]

$$R^* = \frac{2\sigma V_m}{\Delta G_p} \quad [7]$$

where

σ = interfacial energy per unit area;
V_m = the molar volume of the precipitates; and
ΔGp = the molar free energy of precipitate formation, which can be expressed as

$$\Delta G_p = \Delta f_v - \Delta f_\delta \quad [8]$$

where

Δf_v = the chemical free energy driving the phase transformation; and
Δf_δ = the strain energy per unit volume

Nucleation of γ' depends on two major factors: one is the chemical free energy provided by the supersaturation in the matrix, and the other is the interface energy, including surface energy and elastic energy, generated by the lattice mismatch between γ and γ'. Therefore, supersaturation and lattice mismatch are two competing parameters that control γ' nucleation. Higher supersaturation results in the larger molar free energy of formation of the precipitates and, therefore, can form cooling precipitates with a smaller critical nucleus size. Also, the smaller the lattice mismatch between γ' and γ, the lower the interface strain energy and the smaller the critical nuclei size required.

In aging or isothermal precipitation cases, initial supersaturation in the matrix is fixed for a given cooling rate and aging temperature. Thereafter, the supersaturation is decreased with the formation and growth of γ' precipitates during isothermal treatment. However, in cooling precipitation cases, the change of supersaturation is a complex competing process, which includes the supersaturation generation due to the continuous cooling and supersaturation consumption due to γ' nucleation and growth.

Figure 17 schematically shows the effect of cooling rate on γ' formation during quenching. It was previously shown that the higher cooling rate results in more undercooling and, subsequently, more supersatuation buildup. Therefore, a large amount of small-nuclei-size γ' precipitates with a small interparticle spacing are nucleated. On the other hand, fast cooling may suppress the diffusion-controlled γ' growth, even though the interparticle spacing is small and short-distance diffusion is required. That is why a higher cooling rate results in a larger amount of smaller cooling precipitates formed with a smaller interparticle spacing.

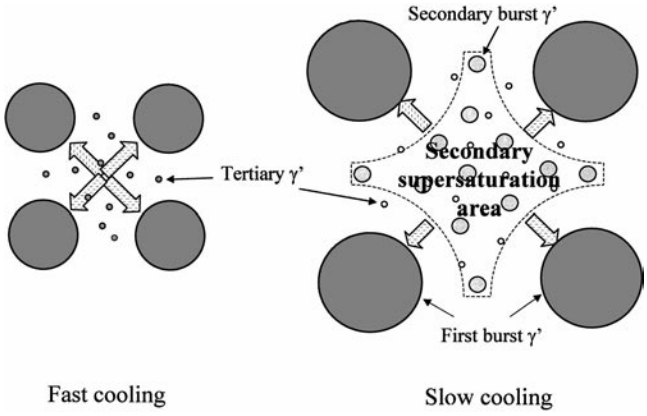

Fig. 17—γ' formation scheme under different cooling rates.

When the cooling rate is lower, the undercooling is less, and, hence, the matrix is less supersaturated. The first-burst γ' precipitates are then bigger and the interparticle spacing is larger. Although the lower cooling rate allows diffusion to occur and, hence, produces larger γ' particles, the long-distance diffusion is unlikely due to the continuous cooling. Therefore, there is a chance for secondary supersaturation to develop again in the vicinity of the first-burst γ' precipitates, because of the continuous cooling. As the secondary supersaturation becomes big enough to overcome the energy barrier for a new round of nucleation, the secondary burst of precipitates becomes possible. This accounts for the double-peak distribution of γ' observed at the slower cooling rate ($<$28 °C/min), as seen in continuous cooling experiments. Since, at that time, the temperature is too low to allow intensive solute diffusion, the growth of the secondary-burst precipitates is restricted. Consequently, the secondary-burst precipitates are much smaller than the first-burst particles. Also, because of the variation of composition in γ and γ' with temperature of formation, it is expected that the secondary-burst γ' particles have a different lattice mismatch from the first-burst ones.[17] This multistage nucleation phenomenon was simulated in the experimental P/M superalloy CH98.[13]

In addition, it is believed that the finest γ' particles, traditionally called tertiary γ' precipitates, are formed during quenching either as secondary-burst cooling precipitates for higher cooling rates or as tertiary-burst cooling precipitates for lower cooling rates. Further investigation using a high-resolution transmission electron microscope (TEM) is required to confirm this.

The results of the interrupt quenching suggest that at the beginning of the quench, nucleation plays a dominant role over a temperature range because of undercooling. After nucleation, the growth of γ' dominates the cooling process until the secondary burst of precipitates occurs. Therefore, the starting cooling rate in the quench process is of much significance in the control of γ' size and the determination of material strength.

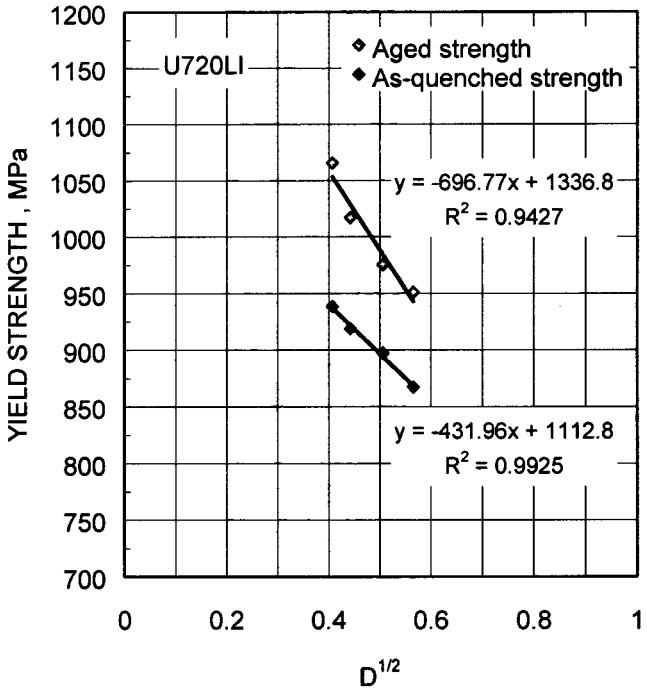

Fig. 18—The yield strength as a function of γ' precipitate size.

B. *Strengthening*

According to the precipitation-hardening theory,[20] when a particle is small, it can be cut or deformed by dislocations or weakly coupled dislocation pairs. There are six properties of the particles that affect the cutting energy: coherency strain, stacking-fault energy, ordered structure, modulus effect, interfacial energy and morphology, and lattice-friction stress. Normally, the summation of these mechanisms leads to an increase in strength with particle size. However, when the particles size increase further, the cutting of particles becomes very difficult, and the dislocations find ways to pass around the particles. When bypass happens, the strength actually decreases with the increase of the particle size. Hence, there is a critical particle size that offers maximum resistance to dislocation motion.

According to the study of U720LI by Jackson,[10] this critical particle diameter, *i.e.*, the particle size for maximum strength, is about 0.04 μm, which corresponds to the separating point between cooling and aging γ' based on the γ' size-distribution charts. According to our experimental results, all cooling precipitates including first- and secondary-burst γ' measured under an SEM are larger than 0.06 μm. Since these particles are larger than the critical size, their strength decreases with a further increase in their sizes. The very fine γ' precipitates are not visible under current SEM examination.

In order to simplify the empirical modelling of mechanical properties, only the first-burst γ' precipitates are considered in the following analysis. This is a reasonable assumption, since only lower cooling rates ($<$28 °C/min) result in a bimodal precipitation-size distribution during quenching. The plot of as-quenched yield strength against the size of the first-burst cooling precipitates formed at different cooling rates in the continuous cooling tests is shown in Figure 18. It was experimentally correlated to a linear relationship between the as-quenched yield strength and square root of the mean diameter of the cooling precipitates, given as

$$\sigma_y = -431.96D^{1/2} + 1112.8 \quad \text{with} \quad R^2 = 0.99 \quad [7]$$

where D is the diameter of the cooling precipitates in microns, and σ_y is the as-quenched yield strength in mega Pascals.

Regardless of cooling rate, the yield strength was observed to increase after aging treatment, as seen in Figure 15. Strengthening due to aging is believed to rely on the growth of the very fine γ' particles. It has been proven that the aging treatment does not cause the secondary cooling precipitates to grow significantly.[10] Hence, it is believed that the main microstructural activity during aging is the continuous growth of the very fine γ' precipitates. Because these particles are smaller than the critical diameter, the strength increases with the increase in the size of those very fine γ' precipitates. However, if the aging time is too long, the size of the fine γ' precipitates crosses the critical value, and overaging and softening occur. It is also noted that the higher cooling rate results in a larger yield-strength increment from aging (shown in Figure 15). A higher cooling rate surpresses the secondary burst of γ' precipitates and provides more supersaturation in the matrix, which results in a greater volume fraction of very fine γ' precipitates formed later on.

The reason for the nonmonotonic decrease of strength with interrupt temperatures is that in the early stages of controlled cooling, first-burst precipitates coarsen and, hence, soften the material. After a certain interrupt temperature, the strength starts to increase with a further decrease in the interrupt temperature. The strengthening effect is believed to be due to the additional fine γ' precipitates burst. These additional γ' precipitates formed are small, strengthening particles. Therefore, the strength increases with the formation and growth of these small precipitates. However, because the volume fraction of these particles is also small, the strength does not increase too much.

The neccessarity of developing a strengthing model that combines the two major mechanisms mentioned previously is obvious because of the multistage bursts of precipitates in U720LI, even though difficulties exist in separating first-burst γ' precipitates from the precipitates formed in later stages, especially from a volume fraction point of view.

II. SUMMARY AND OUTLOOK

The P/M superalloy U720LI was used as a model alloy to investigate the cooling precipitation through controlled cooling procedures. The Thermo-Calc phase-diagram software was employed to estimate the phase transformation through the entire temperature range of interest. The DTA technique was applied to verify the solvus temperature of the γ' phase. The real relationship between the cooling rate and size of cooling precipitates has been studied for U720LI alloys based on the capability of accurately controlling the linear cooling profile through the entire quenching process. The size and the volume fraction of cooling γ' precipitates increase with the decrease in cooling rates. At the cooling-rate range of 11 °C/min to 167 °C/min, the mean diameters of cooling γ' precipitates are around 0.15 to 0.35 μm in U720LI. Of the most significance is the multiple nucleation and resultant binomial distribution of cooling precipitates occurring at cooling rates lower than 27 °C/min. The size

of the first-burst cooling γ' precipitates as a function of cooling rate obeys a power law. The morphology of γ' precipitates changes from a near-cuboidal to an irregular shape because of selective coarsening at lower cooling rates.

Interrupted cooling experiments were performed at specific temperatures to evaluate the progress of precipitation. The growth of cooling precipitates was found to occur continuously from the temperature slightly below the solvus temperature down to 650 °C. The morphology changes from an initial spherical and cuboidal shape to an irregular shape as the interrupt temperature drops to 900 °C. The change is believed to be associated with the coarsening of the precipitates.

Room-temperature tensile properties were measured on specimens quenched at different cooling rates. Tensile tests were also conducted on the specimens in which the quenching process was interrupted at different temperatures during quenching. Both the cooling rate and aging treatment play important roles in strengthening. The yield strength increases with the increase in cooling rate. The aging treatment increases the yield strength by about 90 to 130 MPa. The strength decreases with the interrupt temperature and then increases at 1010 °C. The regaining of strength is believed to be related to the formation of the very fine γ' precipitates. Further TEM examination should be carried out to confirm this theory. A multimodel strengthening mechanism is suggested for future mechanical properties modeling.

This concentrated research effort has explored significant precipitation behavior in the high-strength P/M superalloy Udimet 720LI. Many results have been employed as a database for thermal process simulation on turbine disk processing at Concurrent Technologies Corporation (CTC) and Ladish Co. A solid foundation has been built for further investigation on the multistage precipitation phenomena and strengthening mechanism

ACKNOWLEDGMENTS

This work was funded by the National Center for Excellence in Metalworking Technology, operated by CTC under Contract No. N00140-92-C-BC49 to the United States Navy as a part of the United States Navy Manufacturing Technology Program. It was undertaken as a part of the "Forging Supplier Initiative" project, a joint United States Air Force/ United States Navy initiative focused on reducing the cost of forged aircraft engine components. The authors acknowledge the technical guidance from Mr. Shesh Srivatsa, GE Aircraft Engines (Cincinnati, OH). The authors also thank Li Yang, Undergraduate Student, Computer Science Department, West Virginia University (Morgantown, WV), for her continuous assistance and help in image processing. Special thanks to Diane Schwegler-Berry, National Institute of Occupational Safety and Health (NIOSH, Morgantown, WV), for her patience and technical support with scanning electron microscopy. The authors also acknowledge Matthew Burrius and Bobby Coulter, former Graduate Students, Department of Mechanical and Aerospace Engineering, West Virginia University, for their help with setting up the quench system and software development.

REFERENCES

1. P.R. Bhowal, E.F. Wright, and E.L. Raymond: *Metall. Trans. A*, 1990, vol. 21A, pp. 1709-17.
2. Jian Mao, V.L. Keefer, Keh-Minn Chang, and David Furrer: *J. Mater. Eng. Performance*, 2000, vol. 9 (2), pp. 204-14.
3. R.A. Wallis: *Adv. Mater. Processes*, 1995, Sept., pp. 42kk-42NN.
4. R.A. Wallis and P.R. Bhowal: *Superalloys 1988*, D.N. Duhl, G. Maurer, and S. Antolovich, eds., TMS-AIME, Warrendale, PA, pp. 525-34.
5. Dwaine L. Klarstrom: *Adv. Mater. Processes*, 1996, vol. 4, pp. 40EE-40HH.
6. Jian Mao, Keh-Minn Chang, and David U. Furrer: in *Superalloy 2000*, T.M. Pollock, R.D. Kissinger, R.R. Bowman, K.A. Green, M. Mclean, S.L. Olson, and J.J. Schirra, eds., TMS, Warrendale, PA, 2000, pp. 109-16.
7. N. Gayraud, F. Moret, X. Baillin, and P.E. Mosser: *Euromat Conf.: Materials Development in Rail, Tire, Wing, Hull Transportation*, Genes, Sept. 22–24, 1992, pp. 1225-33.
8. S.T. Wlodek, M. Kelly, and D. Alden: in *Superalloy 1992*, S.D. Antolovich, R.W. Stusrud, R.A. MacKey, D.L. Anton, T. Khan, R.O. Kissinger, and D.L. Klarstrom, eds., TMS, Warrendale, PA, 1992, pp. 467-76.
9. David Ulrich Furrer: *Scripta Mater.* 1999, vol. 40 (11), pp. 1215-20.
10. M.P. Jackson and R.C. Reed: *Mater. Sci. Eng.*, 1999, vol. A259, pp. 85-97.
11. N. Gayraud, F. Moret, X. Baillin, and P.E. Mosser: *J. Phys. III*, 1993, vol. 3, pp. 271-76.
12. S.T. Wlodek, M. Kelly, and D.A. Alden: in *Superalloy 1996*, R.D. Kissinger, D.J. Deye, D.L. Anton, A.D. Cetel, M.V. Nathal, T.M. Pollock, and D.A. Woodford, eds., TMS, Warrendale, PA, 1996, pp. 129-36.
13. Timothy P. Gabb, Daniel G. Backman, Daniel Y. Wei, David P. Mourer, David Furrer, Anita Garg, and David L. Ellis: in *Superalloy 2000*, T.M. Pollock, R.D. Kissinger, R.R. Bowman, K.A. Green, M. Mclean, S.L. Olson, and J.J. Schirra, eds., TMS, Warrendale, PA, 2000, pp. 405-14.
14. Jian Mao, Kelan Yu, and Ruifa Zhou: *Aeronautical Mater.* , 1989, vol. 9 (4), pp. 1-9 (in Chinese).
15. Charles E. Bates and George E. Totten: *Adv. Mater. Processes*, 1991, vol. 3, pp. 25-28.
16. Keh-Minn Chang and Jian Mao: Internal Report, West Virginia University, Morgantown, WV, July 2000.
17. David U. Furrer: Doctorate of Engineering Dissertation, Universitat Ulm, Ulm, Germany, 1999.
18. K. Kusabiraki, Xiao-Min Zhang, and Takayuki Ooka: *Iron Steel Inst. Jpn. Int.*, 1995, vol. 35 (9), pp. 1115-20.
19. H. Wendt and P. Hassen: *Acta Metall.*, 1983, vol. 31 (10), pp. 1649-59.
20. George E. Dieter: *Mechanical Metallurgy*, 3rd ed., McGraw-Hill Co., New York, NY, 1986, p. 215.